ACS APPLIED POLYMER MATERIALS

pubs.acs.org/acsapm

Article

Shear-Induced Stack Orientation and Breakup in Cluster Glasses of Ring Polymers

Maximilian Liebetreu* and Christos N. Likos

Cite This: *ACS Appl. Polym. Mater.* 2020, 2, 3505−3517

Read Online

ACCESS | Metrics & More | Article Recommendations | Supporting Information

ABSTRACT: Cluster glass-phase ring suspensions exposed to weak shear stress exhibit a stable reorientation of stacks as well as of individual ring polymers with the flow direction and into the flow-vorticity plane. The suspension features shear thinning for a variety of different densities as a result. Under strong shear, a breakup of these clusters takes place, accompanied by a subsequent homogenization of the distribution of centers-of-mass of rings, though their orientational preference is maintained. The flow properties of the system are determined by an interplay between the deformability of the constituent particles of the rings and the response of the anisotropic clusters to shear. We employ mesoscopic simulations to investigate and quantify this behavior as well as to provide an explanation for the underlying mechanism, and we show our findings are qualitatively independent of the consideration or disregard of hydrodynamic interactions. After cessation of shear, the system displays strong memory as regards the stack orientation, although individual rings relax into their equilibrium orientation. Potential applications include the possibility to tune the mechanical properties of the material via molecular architecture and rigidity, as well as the flexibility in creating persisting anisotropies in the material as a result of applied shear.

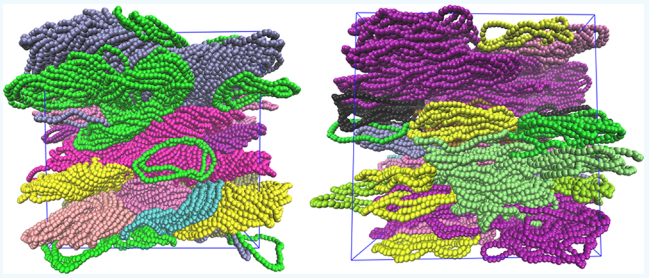

KEYWORDS: *ring polymers, clusters, glass, shear, computer simulation, molecular dynamics, flow, hydrodynamics*

1. INTRODUCTION

In recent years, increasing attention has been dedicated to the behavior of ring polymers in a host of different environments. The topological state of polymers can be controlled by the use of optical tweezers,[1] and it is known that some DNA molecules naturally occur as rings. Examples of the latter include plasmids, circular bacterial chromosomes, mitochondrial DNA as well as the kinetoplast, an interlocked structure of DNA minicircles found in the mitochondria of trypanosome parasites.[2] Moreover, circular single-strand DNA of various contour lengths has been recently successfully prepared by T4-ligase,[3] whereas double-strand DNA rings with sizes of ∼10 nm have been synthesized to produce mechanically interlocked circles in the form of catenanes,[4−6] a class of molecules that has also attracted considerable theoretical interest recently.[7,8] Because of the variety of naturally or synthetically available DNA rings, circular polymers with contour lengths that vary from the order of to many orders of magnitude of the polymer's persistence length are readily available. Accordingly, both long, flexible ring polymers and semiflexible, stiff rings are physical systems whose collective behavior deserves attention.

Considering the simplicity of the topological change of merely connecting two ends of a linear chain, the host of phenomena exclusive to ring-shaped topologies is remarkably novel and rich. Experimental as well as computational research in this area has rapidly gained importance of late. The circular topology of the rings results in a host of unique and fascinating properties in all aspects of structure and dynamics of solutions of such polymers, both in and out of equilibrium. At the dilute limit, hydrodynamics is crucially important. Single-molecule studies have focused on the behavior of rings under specifically imposed external flows.[9−15] It has been established recently that the introduction of a simple topological constraint, namely, connecting the two ends of a full flexible chain, gives rise, for example, to a swelling of the ring along vorticity direction under shear[11] and to an inflation phase for certain shear ranges.[15] Both effects are exclusive to ring-shaped polymers and only appear under the consideration of fully developed hydrodynamic interactions. Hydrodynamic effects like these can be introduced by multiparticle collision dynamics, a stochastic rotation dynamics method that allows particle-based solvent simulation.[16] In highly concentrated solutions and in the melt, hydrodynamics are either screened or altogether absent, and thus the interesting aspects of the problem pertain to the spatial correlations between the rings

Received: May 18, 2020
Accepted: July 2, 2020
Published: July 2, 2020

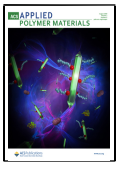

https://dx.doi.org/10.1021/acsapm.0c00522
ACS Appl. Polym. Mater. 2020, 2, 3505−3517

and the mutual arrangement of entanglements in bringing about unusual structural and dynamic behavior. Here, one usually focuses on rings sufficiently long to be considered flexible.[17−19] Recent advances have shed light on the peculiar stress relaxation of ring melts,[20] their response to stretching and elongational flow,[21,22] issues related to mutual threading in ring melts,[23,24] as well as a host of novel phenomena related to dynamical arrest in passive[25] or active ring polymer melts, the latter giving rise to a novel state of matter, termed *active topological glass*.[26] Finally, recent computational studies on the separation of linear chains and rings have been conducted,[27] and the proposed filtering methods make use of the different responses of the two species to external flow fields, depending on topology.[28]

Semiflexible ring polymers are playing an increasingly important role in biotechnology and materials science. Macrocyclic peptides have been recently proposed as drug delivery agents,[29] whereas cyclic poly(phthalaldehyde) has demonstrated promise as a basis for recyclable materials.[30,31] Concentrated solutions of semiflexible rings have been shown to form novel, hierarchically organized, and amorphous cluster phases.[32−34] In these phases, rings form long stacks without long-range translational or orientational order but with strong inter-ring correlations within each stack and across neighboring ones. While the rings forming the stack have an oblate shape, a few others assume a prolate conformation and lie in the stack's interior. Even more unusual is the dynamics of the cluster phase, in which a novel state of arrested matter termed *cluster glass*[35] is formed. This cluster glass features, in stark contrast with common molecular or colloidal glass formers, a separation between self- and collective relaxation dynamics. In particular, while the overall cluster structure is dynamically arrested, individual rings still hop between clusters, giving rise to a system that is ergodic at the level of individual particles, paralleling the phenomena observed in the dynamics of *cluster crystals* that are diffusive at the single-particle level but show long-range order for the clusters themselves.[36]

Colloidal glasses in general are excellent systems to study the structure and dynamics of concentrated suspensions both in the liquid and in the glassy phases. Major advantages they offer over their molecular counterparts are the ability to tune the interactions between their components as well as the mesoscopic sizes of the constituent particles, which facilitate optical observation methods as well as rheological measurements. In (colloidal) glasses, an issue of major importance for the understanding of the distribution of stresses in their interior as well as the processes that affect the shape and lead to the breakup of cages is to study and understand their response under externally imposed shear.[37−41] Whereas our understanding of flow, yield-stress behavior, and structural rearrangements in glasses under shear has significantly advanced in the recent past due to such studies, the investigations have been focusing on cage-forming glasses of spherical colloids. Moreover, and despite active interest in the shear-flow properties of soft, deformable spheres in the glassy region,[38,42−45] the main amount of work has focused on hard and rigid colloids.

The cluster glass formed by semiflexible ring polymers differs markedly from the above-mentioned glass phases on a number of counts: the arrested entities, that is, the stacks, are secondary structures in a hierarchical buildup and not the primary constituents of the solution; the form of the arrested superstructures is anisotropic, and their sizes are polydisperse; the stacks are "living" entities exchanging individual rings with one another even within the glassy regime; and, finally, the elementary building blocks, that is, the semiflexible rings, are deformable objects that adjust their shapes and sizes to the imposed flow, providing thereby an additional mechanism for the material to reorganize itself under the imposed shear stresses.

This work aims at investigating the properties of cluster glasses under steady shear and at providing an understanding of the structural rearrangements occurring in sheared ring suspensions, thereby shedding light on the underlying structure, conformation, and out-of-equilibrium dynamics of such a glassy system under shear flow. Of particular interest is the question of whether or not stacks of rings from the cluster glass phase survive being sheared, and how the orientation of rings relative to each other is modified under flow.

We find that systems across several densities in the glass regime exhibit very similar behavior when sheared. Ring polymer suspensions display shear-thinning behavior, caused mainly by a reorientation and general alignment of rings into the flow-vorticity plane, allowing rings to move in layers stacked on top of each other. More specifically, such semiflexible rings homogenize under strong shear that destroys the equilibrium stacks, a feature reflected in various quantitative measures of spatial uniformity. A much more intriguing effect occurs under weak shear, where stacks from the glass phase can be maintained and align themselves along the flow direction. Simultaneously, the rings still align into the flow-vorticity plane, and the observed stacks consist of many rings that are aligned in parallel but have shifted centers-of-mass with respect to their direct neighbors. We also demonstrate that the system has orientational memory of the shear direction after cessation of the same.

We suggest our results could be used to faciliate a method to develop stacking behavior with a bias to a certain orientation, gained by first shearing a glass-phase system and then allowing it to equilibrate again. Moreover, the properties of the cluster glass both in equilibrium and under flow can be tuned by steering the rigidity of the circular polymers through, for example, screening of the electrostatic repulsions leading to molecular swelling. Bulk simulations are computationally costly, and the consideration of hydrodynamic interactions requires more complicated simulation models. We report here that all observed effects are independent of hydrodynamic interactions for sufficiently concentrated systems in the glass phase.

2. SIMULATION OF CLUSTER GLASS UNDER SHEAR

2.1. Model System. We employed Multi-Particle Collision Dynamics[16,46] (MPCD) to simulate a solvent, a method that fully accounts for hydrodynamic interactions (HI), as well as a well-established adaptation of the same algorithm[11,47,48] that disregards HI to allow for a direct comparison of the findings and assess thereby the role of the latter. A linear velocity profile for the solvent was established by Lees-Edwards boundary conditions[49] at constant temperature in accordance with planar Couette flow, $\mathbf{v}_s(\mathbf{r}) = \dot{\gamma} y \hat{\mathbf{x}}$, where $\dot{\gamma}$ denotes the shear rate, $\mathbf{r} = (x, y, z)$ is an arbitrary position vector, and we define $\hat{\mathbf{x}}$, $\hat{\mathbf{y}}$, and $\hat{\mathbf{z}}$ as the flow-, gradient-, and vorticity directions, respectively. Furthermore, the system is prevented from viscous heating by a Maxwellian cell-level thermostat.[46] To simulate semiflexible rings, we employ molecular dynamics (MD) based on the Kremer-Grest bead−spring model[50,51] with the addition of a

https://dx.doi.org/10.1021/acsapm.0c00522
ACS Appl. Polym. Mater. 2020, 2, 3505−3517

bending potential that accounts for rigidity.[33] The equations of motion for the MD aspect of the simulation are solved by Velocity-Verlet.[52] The monomers are then coupled to the solvent via the MPCD collision step.[16] As we required a large amount of monomers to reach adequate densities and needed to perform those simulations reasonably fast to conduct investigations at a large variety of shear rates, we employed our own code written in C++/CUDA[53] to be run on a graphics processing unit (GPU) cluster. The code has therefore been tested rigorously and has been used successfully in previous works.[11,15]

Following Bernabei et al.[32] and Slimani et al.,[35] we define an effective density $\rho^* = N_R \cdot \langle D_{g,0} \rangle^3 / V$, where N_R is the number of semiflexible rings in the system, V is the volume of our simulation box, which was kept constant at $(50 \times 50 \times 50)a^3$, with a being a unit of length corresponding to the cell length of an MPCD collision cell,[16] and $\langle D_{g,0} \rangle$ is the equilibrium diameter of gyration equal to $\sim 13\sigma$ for a contour length of $N = 50$, with $\langle D_{g,0} \rangle = 2\langle R_{g,0} \rangle$, where σ is the Lennard-Jones length parameter employed for the Lennard-Jones potential, and $R_{g,0}$ is the equilibrium radius of gyration in highly dilute suspension. For this work, we investigated in detail effective densities $\rho^* = \{15.99, 20.04, 26.36\}$, corresponding to $N_R = \{910, 1140, 1500\}$ and monomer densities $\rho = (N_R \times N)/V \cong \{0.364, 0.456, 0.600\}a^{-3}$, respectively. At the highest density, $\rho^* \cong 26.36$, the monomer density $\rho \cong 0.6a^{-3}$ is getting close to a melt. However, the system at hand shows the same qualitative features at lower densities, so we should be adequately below the melt threshold in this work.

In addition to our main investigations for concentrated systems, we also looked at a single dilute one. For this purpose, a run with $N_R = 10$ rings was performed to compare features of semiflexible versus flexible ring behavior in highly dilute solution, where HI is crucial. For this case, we have an effective density $\rho^* \cong 0.18$ and a monomer density $\rho \cong 0.004a^{-3}$.

All other parameters for our simulation were adjusted to reproduce as closely as possible the glass-phase behavior studied by Poier et al.;[33] therefore, we limit our investigation to a single value for the rigidity constant, $\kappa_B = 30.0k_BT/\epsilon$. All rings employed are unknotted, which is also physically expected for this value of the rigidity and the ensuing moderate value of contour-to-persistence length ratio of the rings.[33]

We chose standard MPCD parameters[16,46] with solvent particle mass $m = 1.0$, $a = \sigma$, and collision angle $\alpha = 130°$. Additionally, we set the amount of solvent particles per collision cell to $\langle N_c \rangle = 10$ and subsequently chose a monomer mass $M = m\langle N_c \rangle$. The time step for MPCD is $h = 0.1[(k_BT)^{-0.5}m^{0.5}a]$, and the time step for MD was chosen as $\delta t = 0.002[(k_BT)^{-0.5}m^{0.5}a]$. These choices result in a solvent viscosity of $\eta_s \cong 8.70[(k_BT)^{0.5}m^{0.5}a^{-2}]$.

2.2. Quantitative Tools. With the MD parameters described before, the resulting relaxation time for a single, isolated semiflexible ring at contour length $N = 50$ is $\tau_{R,0} \cong 11\,500[(k_BT)^{-0.5}m^{0.5}a]$ with HI and $\tau_{R,0} \cong 45\,500[(k_BT)^{-0.5}m^{0.5}a]$ without HI. To obtain these values, we define the autocorrelation function $\Phi(t)$.[54]

$$\Phi(t) = \frac{\langle \mathbf{R}_e(t) \cdot \mathbf{R}_e(0) \rangle}{\langle \mathbf{R}_e^2 \rangle} \tag{1}$$

For a linear chain, $\mathbf{R}_e$ would be the end-to-end vector. For a ring, it can be defined as the vector from any bead i to the opposite bead $(i + N/2)$ modulo N. The arbitrary choice of a bead i must be taken into account when averaging. We then fit $\Phi(t)$ with a function $f(t) = a_0 e^{-t/\tau_1} + (1-a_0)e^{-t/\tau_2}$ and finally obtain the relaxation time $\tau_{R,0}$ from integrating the fitting function $f(t)$.[54]

$$\tau_{R,0} = \int_0^\infty f(t)\, dt = a_0\tau_1 + (1 - a_0)\tau_2 \tag{2}$$

We can then define a variant of the Weissenberg number $Wi_0 = \dot{\gamma}\tau_{R,0}$,[55,56] which takes the relaxation time of a semiflexible ring in a dilute system as the reference point, rather than the relaxation time $\tau_R(\rho)$ at finite concentration; the latter can be significantly higher than $\tau_{R,0}$ for dense systems.[57]

To describe the general shape of individual ring polymers, we employ the gyration tensor G,[58] defined as follows

$$G = \frac{1}{N}\sum_{i=1}^{N} \mathbf{s}_i \otimes \mathbf{s}_i \tag{3}$$

where $\otimes$ is the dyadic product, and $\mathbf{s}_i$ is the position of bead i on a ring of contour length N relative to the ring's center-of-mass $\mathbf{r}_{CM}$ such that $\mathbf{s}_i = \mathbf{r}_i - \mathbf{r}_{CM}$.

The gyration tensor has a number of useful properties for analyzing an object's shape and orientation in space. First, we will require eigenvalues and the corresponding eigenvectors of G. We label the eigenvalues λ_k such that $\lambda_1 \geq \lambda_2 \geq \lambda_3$ and the eigenvectors $\hat{e}_1, \hat{e}_2, \hat{e}_3$ to match their corresponding eigenvalues. Then, $\hat{e}_1$ corresponds to the first principal component, indicating the direction of the main extension of the ring. Orthogonal to it, but still in the plane of the disklike ring, we find $\hat{e}_2$. Orthogonal to both and therefore orthogonal to the plane in which the disklike ring resides is $\hat{e}_3$, which we term director $\mathbf{d}$ in the context of this work.[34,59]

The eigenvalues of G add up to the instantaneous squared radius of gyration.

$$R_g^2 = \lambda_1 + \lambda_2 + \lambda_3 \tag{4}$$

Let $\langle \cdots \rangle$ denote the time-average expectation value of a quantity. Apart from the evident radius of gyration $\langle R_g^2 \rangle$, the following shape parameters are of use.[58,60]

First, we define prolateness $S^* \in [-0.25; 2]$, which measures how much the object at hand ressembles an ellipsoid.

$$S^* = \left\langle \frac{(3\lambda_1 - R_g^2)(3\lambda_2 - R_g^2)(3\lambda_3 - R_g^2)}{R_g^6} \right\rangle \tag{5}$$

The acylindricity $c = \langle \lambda_2 - \lambda_3 \rangle$ can be normalized with $\langle R_g^2 \rangle$, and we obtain $c/\langle R_g^2 \rangle \in [0;0.5]$, where $c/\langle R_g^2 \rangle = 0$ in the case of cylindric symmetry of the object at hand (with $\lambda_2 = \lambda_3$).

Similarly, we can define the deformational resistance m_G as

$$m_G = Wi_0\left(\frac{2\langle G_{xy} \rangle}{\langle G_{xx} \rangle - \langle G_{yy} \rangle}\right) \tag{6}$$

where Wi_0 is the Weissenberg number as computed from $Wi_0 = \tau_{R,0} \cdot \dot{\gamma}$.

We also require computation of the polymeric viscosity η of the solution. We employ the stress tensor $\sigma_{\alpha\beta}$ according to the modified Kramers expression[61]

$$\sigma_{\alpha\beta} = \sum_{i=1}^{N} \langle \mathbf{s}_{i,\alpha}\mathbf{f}_{i,\beta} \rangle \tag{7}$$

https://dx.doi.org/10.1021/acsapm.0c00522
ACS Appl. Polym. Mater. 2020, 2, 3505−3517

where $\mathbf{f}_i$ is the total force acting on bead i. The polymeric viscosity can then be written as[62]

$$\eta = -\frac{\sigma_{xy}}{\dot{\gamma}} \tag{8}$$

where $\hat{x}$ is the flow direction, and $\hat{y}$ is the gradient direction.

To detect stacks of rings we employ the ring directors $\mathbf{d}_i$ following the approach chosen by Bernabei et al.[32] as well as in subsequent works.[34,35] A ring j is considered on the same stack as ring i if the following criteria are fulfilled[34]

$$\begin{aligned} \left|\left|\mathbf{d}_i \cdot \mathbf{d}_j\right|\right| &\geq 1 - \Delta\gamma \\ \left|\left|\mathbf{r}_{ij} \cdot \mathbf{d}_i\right|\right| &\leq v_{\parallel} \\ \left|\left|\mathbf{r}_{ij} - \mathbf{d}_i \cdot (\mathbf{r}_{ij} \cdot \mathbf{d}_i)\right|\right| &\leq v_{\perp} \end{aligned} \tag{9}$$

where $\mathbf{r}_{ij}$ denotes the distance between the centers-of-mass of both rings i and j, and $\Delta\gamma$, $v_{\parallel}$, and $v_{\perp}$ are parameters to be chosen a posteriori.

Note that $\|\mathbf{d}_i\| = 1$, so the first criterion limits the angle between two directors, while $v_{\parallel}$ indicates how far apart two centers-of-mass can be parallel to each other's directors, and $v_{\perp}$ indicates how far misaligned centers-of-mass from the same stack can be orthogonal to each other's directors. Poier et al.[34] suggest values of $\Delta\gamma = 0.1$, $v_{\parallel} = 3.0\sigma$, and $v_{\perp} = 2.5\sigma$ for semiflexible rings at $N = 50$ in agreement with our model, so we opted to use the same parameters and confirmed their usefulness for the system at hand a posteriori by looking at the highlighted stacks and finding good agreement with intuitive assignment.

To measure uniformity and clustering behavior, we chose remoteness $P(d)$[63,64] and dispersion index (DI), the former suggested to be used in the context of particles, for example, by Gompper et al.,[65] the latter previously discussed for studies of clusters by Kam et al.[66] Both parameters require the introduction of a cubic lattice of cell length l into the simulation box. We found a choice of $l = 1.0a$ for $P(d)$ and of $l = 2.5a$ for DI to result in smooth graphs. The obtained numerical values are interpreted mostly in comparison to each other.

The remoteness $P(d)$ is the distribution of distances d from each lattice point to the nearest particle. As such, $P(d)$ might peak at different values across different densities, and the height of this peak is similarly affected. A sharper peak of the distribution indicates uniformity and the absence of large voids or clusters from the system, but only when interpreted relative to a reference system. Here, we investigate $P(d)$ for centers-of-mass instead of particles and find good agreement with visual observation and measured stack lengths h_c.

In addition to the remoteness, we also employ, as a quantitative tool for the characterization of clustering, the dispersion index of the system.[66] This quantity is defined as DI $= s^2/\mu$, where s is the sample standard deviation, and μ is the sample mean for center-of-mass counts per lattice cell. A dispersion index close to 1 means particle distribution across the lattice resembles a Poisson-random distribution. A value DI > 1 indicates clustering, and a value DI < 1 indicates a stronger uniformity than the one expected from an uncorrelated (Poisson) distribution of particles. Here, we investigate DI not for particles but for centers-of-mass. The remoteness $P(d)$ and the dispersion index are complementary tools. Whereas $P(d)$ as a distribution provides more detailed information than the DI, its peak is meaningless, as is its width: both depend on the choice of grid constant l and the density in the system. The remoteness cannot indicate clustering by itself; it can only suggest more or less clustering relative to another system. Additionally, plotting many remoteness distributions together makes for a messy plot. The DI provides a measure for clustering that can be measured against a value of reference, namely, the value 1, at which particles are randomly distributed inside the simulation box, allowing comparison of different systems and concise graphs. To justify the use of DI, we show also $P(d)$ and cumulative stacking probability $p(h_c)$ in Figure 2 and confirm that $\langle \mathrm{DI} \rangle$ (see Figure 3a) shows the same features as obtained from $P(d)$ and $p(h_c)$.

3. RESULTS AND DISCUSSION

3.1. Clustering Behavior. In equilibrium, semiflexible ring polymers form stacklike clusters as a glass phase.[32,33,35] We reiterate that this is not a glass in which each individual monomer is arrested: indeed, the monomer packing fraction is not sufficiently high for that purpose. It is rather an arrested state for the collective arrangement of the rigid rings as entire objects, as expressed by the fact that the coherent (collective) density autocorrelation function has a long time plateau. The reason for this arrest is the organization of the rings into long clusters, brought about by the overall steric and rigidity constraints and the intercalated nature of these clusters, which makes them extremely slow in relaxation. An additional peculiarity of this cluster glass, which underlines its distinct character with respect to the usual polymer glasses, is the decoupling between coherent and incoherent density autocorrelation functions: although the former remains arrested, the latter relaxes due to individual ring hopping between different clusters. We were able to reproduce these configurations in our equilibrium simulations. The behavior under shear, however, had not been investigated before.

First, we present some visual evidence in Figure 1. Comparing panels 1a−c, from near-equilibrium to strongly sheared system, we can clearly see marked structural changes taking place. For one, near equilibrium (Figure 1a), stacks are oriented randomly with a slight but insignificant bias due to the long-range correlation from individual clusters forming. A typical stack features several rings with similar orientation (and some rings threading the others, orthogonal to the rest of the stack), and rings on the stack are oriented such that their directors $\mathbf{d}$ are parallel to the stack itself. Under shear, that is no longer true (Figure 1b). In weak shear flow, stacks form linear bands aligned in the flow direction, and the resulting configuration of stacks of rings flowing in parallel to each other is stable over several relaxation times $\tau_{R,0}$. Moreover, rings on each stack are no longer oriented similarly to but instead are strongly tilted with respect to the stack itself. Under strong shear (Figure 1c), stacks do not align anymore, but rather are rapidly destroyed, with shear causing the rings to move through the simulation box homogeneously distributed. Under these conditions, stacks are almost always detected orthogonal to the flow axis, which is partly due to all rings being aligned in the flow-vorticity plane. The resulting stacks as recognized by the employed algorithm are most often short and coincidental and might look quite different from one analyzed frame to the next.

A more thorough insight can be gained from Supporting Videos S1−S5, which show centers-of-mass in the system without hydrodynamic interactions, for flow-gradient perspec-

https://dx.doi.org/10.1021/acsapm.0c00522
ACS Appl. Polym. Mater. 2020, 2, 3505−3517

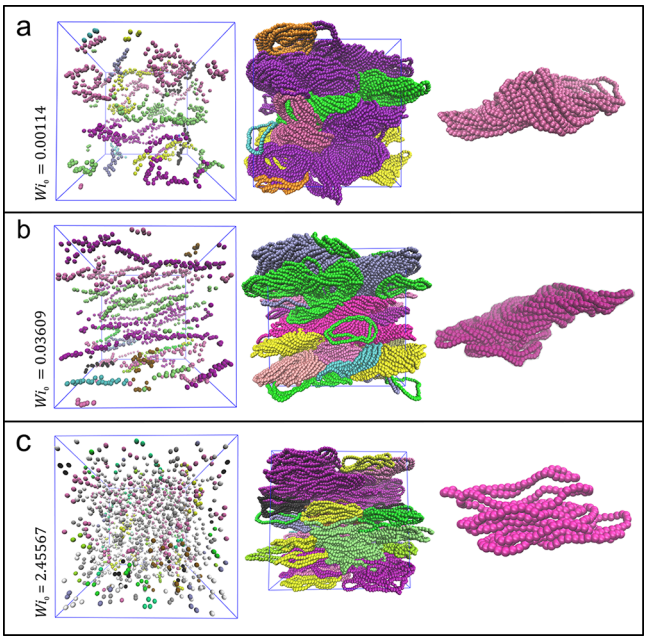

Figure 1. Snapshots of semiflexible rings in the bulk under shear. Snapshots taken with VMD[67] at effective density ρ^* = 26.36, which are also representative for the remaining two effective densities ρ^* = 15.99 and ρ^* = 20.04. Rings on the same stack are shown in the same color to indicate allegiance (but not always in the same color scheme in each panel, and the same color might appear several times for different stacks in the same panel). All panels are structured in the same way and seen in flow-gradient view. (left to right) Centers-of-mass of all stacks with $h_c \geq 5$ (with the exception of panel (**c**), where the left-most picture shows centers-of-mass for all rings in the simulation box to emphasize the random distribution of rings and the breakup of stacks; here, rings belonging to a stack of one or two rings are colored white and silver, respectively); stacks of rings with $h_c \geq 5$; and a typical stack at that shear rate. (**a**) Near-equilibrium system at Wi_0 = 0.001 14. (**b**) System under weak shear at Wi_0 = 0.036 09. (**c**) System under strong shear at Wi_0 = 2.455 67.

tive and increasing shear rates. Supporting Video S1 shows a plain, equilibrium configuration, and Supporting Videos S2−S4 feature the aforementioned linear bands, while Supporting Video S5 shows the chaotic behavior at strong shear. The reader is referred to the Supporting Information section for detailed descriptions of all videos.

The observations from visual inspection are readily quantifiable by applying proper morphometric measures to describe the structure of the system. As the reorganization encompasses features going beyond pair structure, we employ tools that are complementary to the usual pair distribution function to follow. One property that describes spatial organization is the remoteness $P(d)$,[63,64] which we can apply to the centers-of-mass of all rings. The result is shown in Figure 2a−c. We can use the distribution of remoteness as an indication of structure homogeneity, where a comparatively broader distribution indicates a more disperse, open structure, and a sharper peak indicates a more uniform distribution at constant density, argued via the (dis)appearance of large voids in the system. Figure 2a−c shows a clear disappearance of voids for increasing shear independent from density, by a more peaked distribution of remoteness $P(d)$.

In Figure 2d−f we show the (cumulative) probability $p(h_c)$ to find any one ring as part of a stack with size (number of rings on that stack) equal to or smaller than h_c. The quantity $p(h_c)$ is calculated as

$$p(h_c) = \left\langle \sum_{n=1}^{h_c} \frac{n \cdot N_n}{N_R} \right\rangle \tag{10}$$

which already keeps $p(h_c)$ in the range of $[0; 1]$, where N_n is the number of stacks of length n, and N_R is the total number of rings in the system. Similarly to the remoteness, we verify that stacks of large lengths are stable at weak shear rates, whereas they destabilize at strong shear. This behavior is independent of density and insensitive to the inclusion of hydrodynamic interactions.

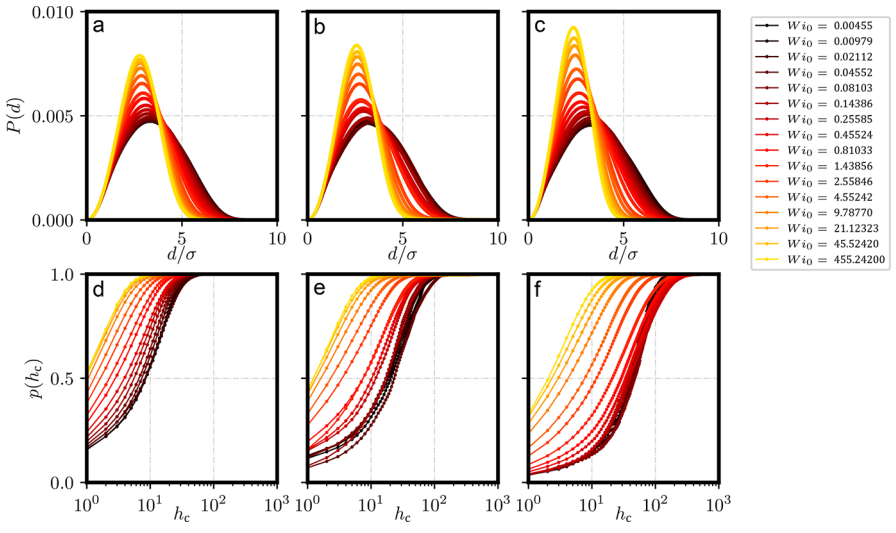

Figure 2. Remoteness and cumulative probability for a ring on a given stack. (**a**−**f**) Increasing effective density ρ^* from left to right: ρ^* = {15.99 (**a**, **d**), 20.04 (**b**, **e**), 26.36 (**c**, **f**)}. All results from runs without hydrodynamic interactions. (**a**−**c**) Distribution of remoteness $P(d)$ against distance d for different Wi_0 values. Distributions have consistently sharper peaks at high shear, hinting at the absence of large voids in these regimes. (**d**−**f**) Cumulative probability $p(h_c)$ for a ring to be part of a stack of length less than or equal to h_c. Stacks of high length become unlikely for strong shear. The result at equilibrium is consistent with that presented by Poier et al.[33]

https://dx.doi.org/10.1021/acsapm.0c00522
ACS Appl. Polym. Mater. 2020, 2, 3505−3517

To further support our observation of breaking of clusters under high shear and our investigation of structure (see also remoteness $P(d)$ in Figure 2a−c), we study the dispersion index of centers-of-mass in the system. As DI ≤ 1 indicates a propensity toward uniform (strongly uniform for DI $\ll 1$) distribution of particles, Figure 3a shows that clusters are broken and vanish for high shear, which is in line with sharper peaks of remoteness (Figure 2a−c) and shorter detected stacks (Figure 2d−f). From DI especially, we can see that rings at strong shear are indeed distributed randomly throughout the simulation box, which is in line with our observations from Figure 1c and Supporting Video S5. Moreover, the three regimes A, B, and C, which we show here, pertain to the clear regimes seen in Figure 7 for individual ring orientations. We show them here already to allow for a later comparison. For now, we encourage the reader to revisit Figure 2 and Figure 3 when we turn to individual ring orientations.

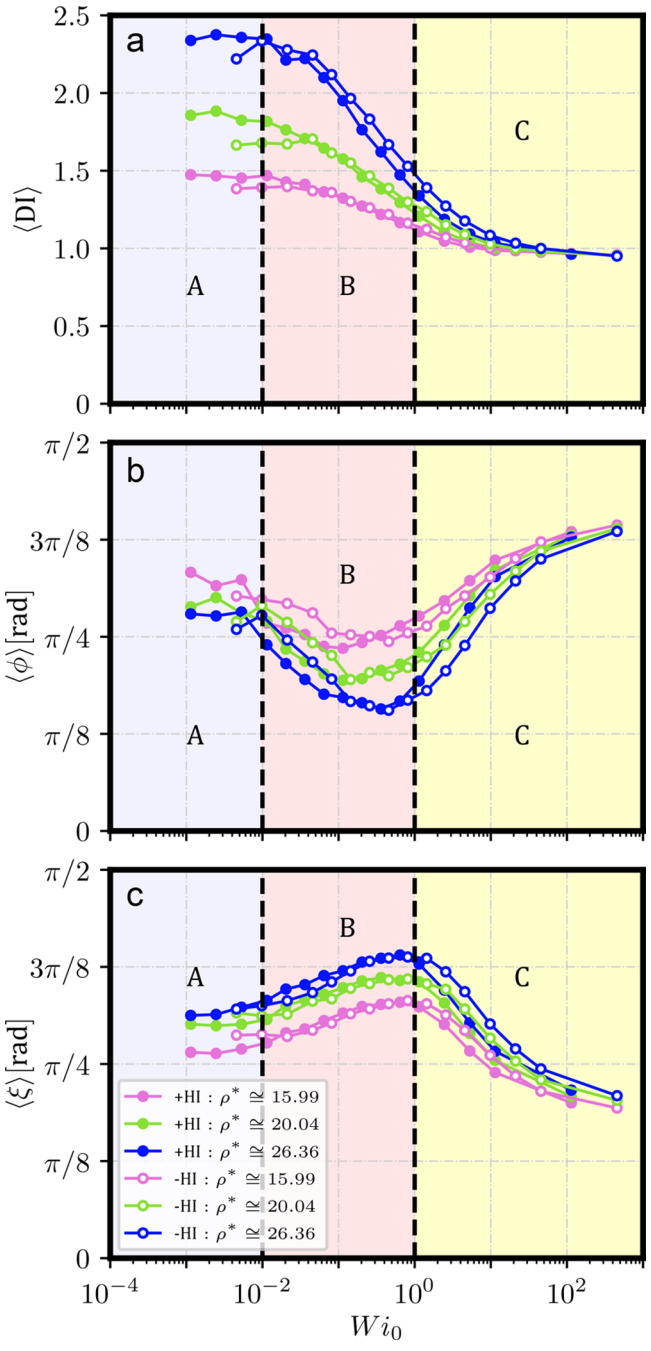

Figure 3. Clustering and stack orientation. (**a**) ⟨DI⟩ decreases with increasing Weissenberg number Wi_0. (**b**) Average angle $\langle\phi\rangle$ of regression fit through all centers-of-mass on a stack to flow axis with increasing Weissenberg number Wi_0. (**c**) Average angle $\langle\xi\rangle$ of regression fit through all centers-of-mass on a stack to individual directors **d** of rings on that stack with increasing Weissenberg number Wi_0.

3.2. Cluster Reorientation. Figure 3b shows the average angle $\langle\phi\rangle$ of the main principal component of all centers-of-mass on a stack (which corresponds to a regression fit) to the flow axis. $\langle\phi\rangle$ is therefore a measure of cluster orientation, but there is a caveat. Under strong shear, only small stacks are stable, and their occurrence is rather random (see Figure 2d−f). Such small stacks are unlikely to be oriented in flow direction by definition, since we constrained the possible shift orthogonal to a ring's director to still be considered part of the same stack. All rings under shear tend to align into the flow-vorticity plane and in parallel to each other as seen in Figure 1c (as well as in Figure 4 and Figure 7, respectively).

The behavior seen in Figure 3b at high shear is therefore more of an artifact of the employed stack detection algorithm. At low shear, however, the observed aligning of stacks is confirmed nicely by the graph, and panel 3b gives us a good indication for when stacks start breaking due to shear: this would have to be around the minimum of $\langle\phi\rangle$. Indeed, checking back with Figure 2d−f, the shear rates around the minima in Figure 3b are also where $p(h_c)$ starts to change pronouncedly from its equilibrium configuration.

We also investigated the orientation of rings to the stack they belong to. To this end, we take the main principal component of the stack (as already used for $\langle\phi\rangle$ before) and measure its average angle $\langle\xi\rangle$ to the individual directors $\mathbf{d}_i$ of each ring on that stack. The result is shown in Figure 3c. As stacks align with the flow direction, so, too, do the individual rings. The dependence of the quantity $\langle\xi\rangle$ on shear rate shows that rings tend to be tilted away from the orientation of their stack with increasing shear, until the aforementioned breaking of clusters and shortening of stacks influences the quantity enough to favor more and more parallel orientations.

In the context of clustering and cluster orientation, let us now consider the orientation of rings relative to each other. Figure 4 shows the correlation of angles between directors and the distance between the respective rings' centers-of-mass. Intuitively, Figure 4 confirms that there is no visible correlation at high distances for very low density $\rho^* \cong 0.18$, more or less independent of shear strength. However, in panel 4m, we see a lingering correlation even at high distances. We will confirm in Figure 7 that this is because of the imposed orientation of individual rings due to shear. In either case, the effect is not very pronounced here for very low density, but it is exceedingly prominent for higher densities ρ^*. We display here the pair distribution function up to distances of $3\langle R_{g,0}\rangle$, which is already fairly far in the direction indicated by the director **d**. The correlation is measured up to half the length of our simulation box, $r_{max} = 25\sigma$.

Weak shear leads to a decrease of the correlations between directors at large distances, compared to equilibrium. We suggest this is because the soft, forced movement allows rings to reach positions where they are more free to orient themselves however their immediate surroundings dictate. We also suggest the long-range correlation at equilibrium

https://dx.doi.org/10.1021/acsapm.0c00522
ACS Appl. Polym. Mater. 2020, 2, 3505−3517

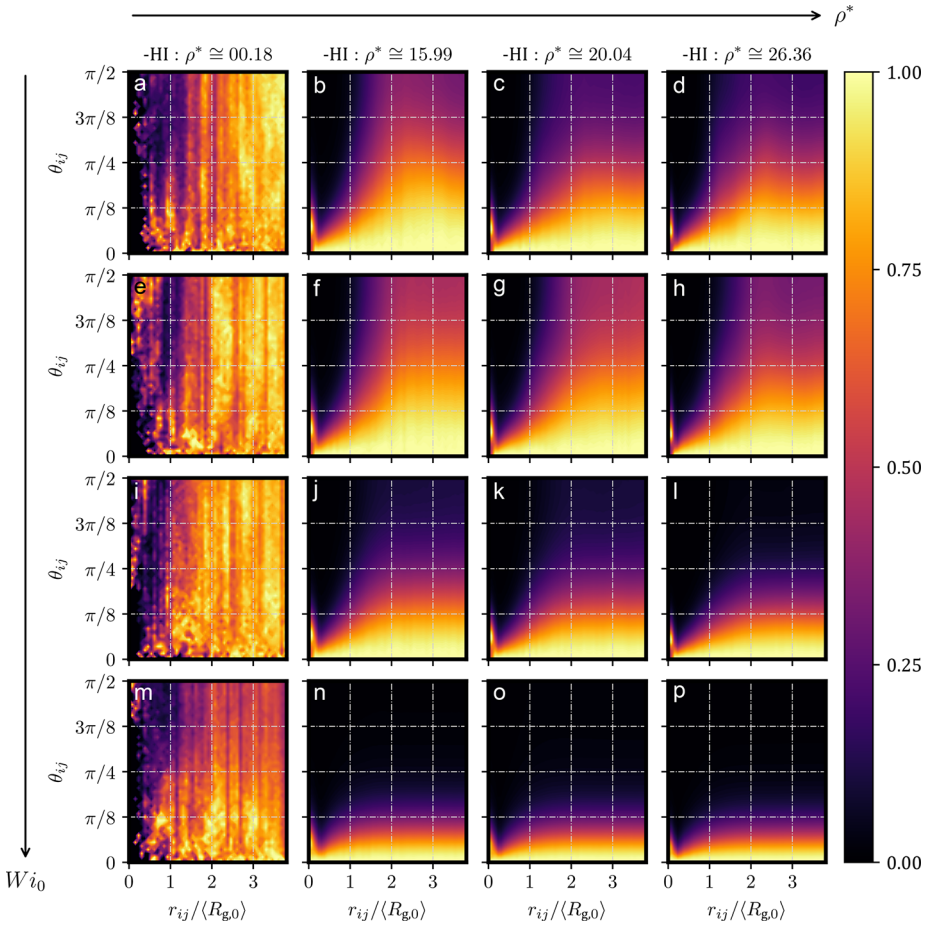

Figure 4. Distribution of angles θ_{ij} between directors $\mathbf{d}_i$, $\mathbf{d}_j$ against distance r_{ij}. The color corresponds to the relative frequency at each distance, with a value of 1 (bright yellow) indicating the most popular angle at a given distance. The vaster the color difference at a certain distance, the more there is a preference toward a certain angle. (top to bottom) Increasing Weissenberg numbers Wi_0 = {0.0046, 0.0455, 0.4552, 4.5524}. (left to right) Increasing densities ρ^* = {0.18, 15.99, 20.04, 26.36}. All results shown here were obtained without HI.

stems from whichever stack forms first, influencing the possible orientation of all other stacks, as well as, subsequently, the rings on it.

For high shear, however, we find all rings to be parallel to each other independent of distance. This is an important insight into the overall configuration of the system, and we can already assume this to influence system rheology (see Figure 5). Furthermore, we find that, across all shear rates and (sufficiently high) densities, rings very close to each other will orient at a slight tilt, while at $\sim 0.3\langle R_{g,0}\rangle$, rings essentially orient in parallel. From this, we surmise that the combination of crowding and the steric constraints leads to slight displacements and tilts of two immediately neighboring rings, but if rings are a certain distance apart, it is almost guaranteed they will be oriented in parallel—a preference that is persistent for dense systems at strong shear.

3.3. Rheology. As all rings increasingly align in parallel to each other (Figure 4) and orthogonal to gradient axis $\hat{\mathbf{y}}$ (Figure 7b) with growing shear rate, they can slide on top of each other. This forced alignment, which actually makes the rings deflate and twist to match the little space they have (see Figure 6), results in a decrease in polymeric viscosity η with increasing shear as seen in Figure 5. Thus, the system experiences shear thinning pronounced enough to turn the very viscous, glassy system at equilibrium into a flowing system at high shear, at which point η gets within 1 order of magnitude of the solvent

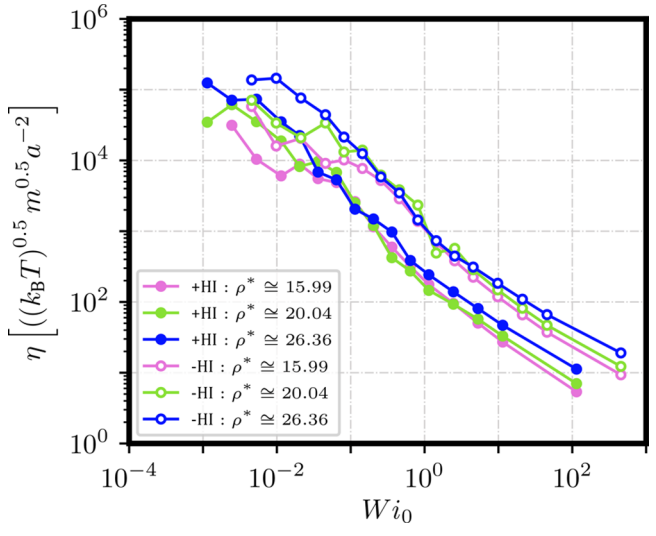

Figure 5. Polymeric viscosity η against Wi_0. Shear thinning is qualitatively independent of density and hydrodynamic interactions.

viscosity η_s. The overall behavior of the viscosity is similar to that seen in hard colloidal glasses.[41,68] However, contrary to the findings for hard sphere glasses, the viscosity versus shear rate curve is not a single power law. There is a slight change of behavior at $Wi_0 \cong 1$, where the system at hand changes its

https://dx.doi.org/10.1021/acsapm.0c00522
ACS Appl. Polym. Mater. 2020, 2, 3505−3517

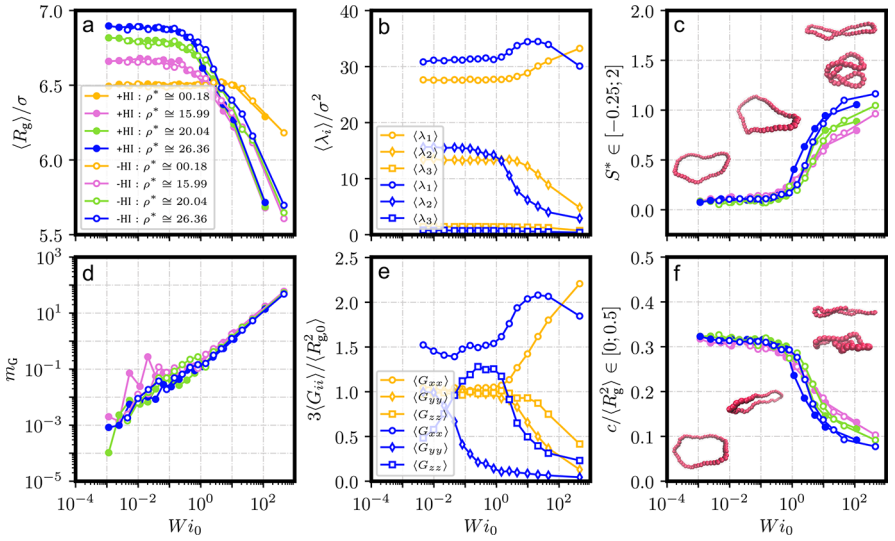

Figure 6. Shape parameters of a semiflexible ring in bulk systems under shear. All parameters[60] are plotted against Weissenberg number Wi_0.[55] Color-coding is maintained as well in panels (**b**, **e**), though symbols differ. (**a**) Radius of gyration $\langle R_g \rangle$. As reference, $\langle R_g \rangle$ in a dilute system at $\rho^* \cong 0.18$ is also shown and matches well the equilibrium values shown in previous works.[32,33] (**b**) Eigenvalues $\langle \lambda_i \rangle$ of the gyration tensor G with $\lambda_1 \geq \lambda_2 \geq \lambda_3$. (**c**) Prolateness $S^* \in [-0.25; 2]$. This panel also shows typical ring configurations (viewed from gradient direction) at the corresponding Wi_0 ranges. (**d**) Deformational resistance m_G. (**e**) Diagonal elements $\langle G_{ii} \rangle$ of the gyration tensor G, normalized via equilibrium radius of gyration $\langle R_{g,0} \rangle$. (**f**) Normalized acylindricity $c/\langle R_g^2 \rangle \in [0;0.5]$. This panel also shows typical ring configurations (viewed from vorticity direction) at the corresponding Wi_0 ranges.

internal structure from one of the oriented clusters to the state in which the clusters have completely dissolved and individual rings distribute themselves homogeneously throughout the solution. Whether the homogeneous system is about to reach a second Newtonian plateau at even higher shear rates[39] cannot be judged from the available data.

3.4. Behavior of Individual Rings. Semiflexible ring polymers under shear exhibit a behavior distinct from that of their fully flexible counterparts: the radius of gyration $\langle R_g \rangle$ decreases with increasing shear. This behavior was confirmed independently before for isolated rings,[69,70] though here we find it is enhanced by a dense system of rings as shown in Figure 6a. The equilibrium radius of gyration $\langle R_{g,0} \rangle$ is also known to increase with density for dense systems due to entropic reasons: shrinking semiflexible rings demand an increase in bending energy, and so threading and clustering are energetically favorable solutions that ultimately lead to the observed swelling.[32] We confirm the known behavior of the radius of gyration $\langle R_g \rangle$ under shear in Figure 6a. The observed shrinking of the ring is caused by an increase in tumbling for dilute systems and magnified for high-density systems by the rings additionally twisting and folding to make up for the imposed stretching due to shear and the energetically favorable clusters being forced to deform. The decrease in $\langle R_g \rangle$ starts to occur at shear rates where stacks start to break apart—at approximately $Wi_0 \cong 10^{-1}$ (see also Figure 2)—and rings are forced to be distributed more uniformly (see Figure 3a).

Of particular interest is the behavior of eigenvalues $\langle \lambda_i \rangle$ in Figure 6b and diagonal gyration tensor elements $\langle G_{ii} \rangle$ in Figure 6e, shown here only for a highly dilute suspension without hydrodynamic interactions at $\rho^* \cong 0.18$ and a concentrated solution at $\rho^* \cong 26.36$ in order not to overcrowd the figure. The other investigated high densities with and without hydrodynamic interactions show the same qualitative behavior as the solution at $\rho^* \cong 26.36$. For both densities, $\langle \lambda_3 \rangle$ remains very small and decreases with shear, which is typical for "planar" molecules. $\langle \lambda_2 \rangle$ starts out close to $\langle \lambda_1 \rangle/2$ and then decreases rapidly for increasing shear, while $\langle \lambda_1 \rangle$ increases marginally before decreasing as well. No such effect is observed for the dilute suspension, indicating crowding to be responsible.

This ties in with what was previously mentioned about the radius of gyration of semiflexible rings.[32,69,70] Here, we suggest rings lack sufficient space to open under high shear, where the more uniform distribution is also not the most energetically favorable. Consequently, the rings twist and fold unto themselves to adjust to their environment.

Similarly, the diagonal gyration tensor elements $\langle G_{ii} \rangle$ differ significantly between dilute and dense suspensions. In a dilute system, rings can move around freely, and so there is no visible spatial preference. As shear increases, the rings stretch along flow direction and deflate in vorticity direction, while also aligning into the flow-vorticity plane. At high densities, an orientational preference is unavoidable due to spatial restrictions. This preference can be seen here, as normalized values of $\langle G_{xx} \rangle$ and $\langle G_{zz} \rangle$ differ significantly from 1 near equilibrium. Note that this orientational correlation could be prevented by averaging over several equilibrated systems, but because we are concerned with how such a system develops under shear, we can neglect gathering more data at equilibrium.

Because the sheared system is in constant turmoil and rings have very limited space to move, their deformational resistance m_G increases as well, as seen in Figure 6d. Note that the slope of $\cong$1 for high Wi_0 indicates a near-constant alignment angle, which is confirmed in Figure 7a–c. Additionally, we see acylindricity c decreasing (the polymers become more cylindrical, Figure 6f), which hints at the polymer overall getting stretched and behaving more like a rod. This agrees well with increasing prolateness S^* (Figure 6c). Supporting Videos S6–S13 show the overall shape and orientation of these rings for a variety of densities and shear rates. We chose to

https://dx.doi.org/10.1021/acsapm.0c00522
ACS Appl. Polym. Mater. 2020, 2, 3505−3517

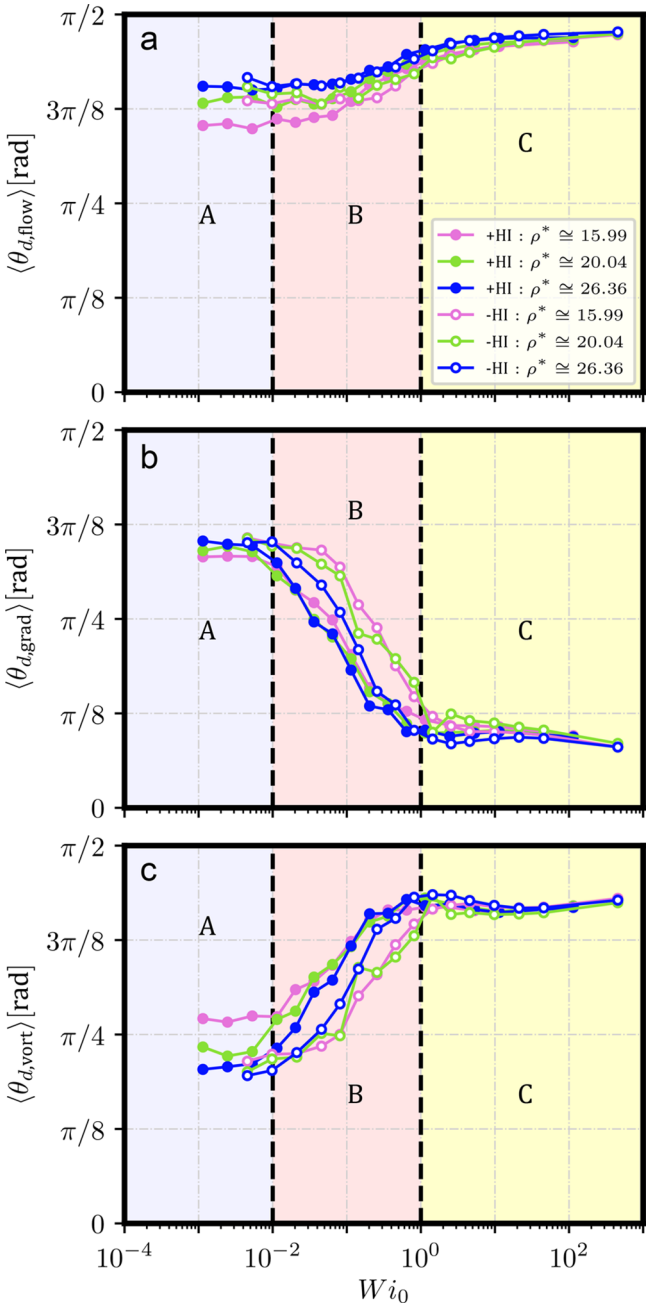

Figure 7. Alignment of semiflexible rings under shear. Average angle $\langle\theta\rangle$ between directors **d** of semiflexible rings and flow (**a**), gradient (**b**), and vorticity (**c**) axes. Across all densities, rings consistently align themselves into the flow-vorticity plane at high shear. The three regimes A, B, and C highlight the orientational changes with shear.

single out rings and track their configuration over time for the creation of these videos.

On the basis of the above evidence, we can now identify three collective structural regimes: A (equilibrium, cluster glass: $Wi_0 \lesssim 10^{-2}$); B (reorientation: $10^{-2} \lesssim Wi_0 \lesssim 10^{0}$); and C (stable, forced orientation: $Wi_0 \gtrsim 10^{0}$). The response of individual rings through orientation can be separated into these same regimes as shown in Figure 7a−c. Note that these regimes seem to align quite well with the transition of stacks from cluster glass, to deformation and reorientation of stacks, to breaking of clusters as shown in Figures 2 & 3.

Semiflexible rings under shear also tend to align themselves into the flow-vorticity plane as shown in Figure 7. All of Figure 7a−c together shows the preferred alignment of the ring director **d** to be parallel to the gradient axis $\hat{\mathbf{y}}$ (Figure 7b). Notably, there is a plateau for high shear rates (regime C) at approximately $\langle\theta_{d,\,\mathrm{grad}}\rangle \leq \pi/8$, indicating strong resistance to further alignment. We suggest this is caused by the high density and by the rings overlapping and preventing each other from orienting themselves perfectly. In addition, note that here we are measuring an angle to an axis, where slight tilts are emphasized because of the cosine dependence. The constant angle at high shear causes deformational resistance m_{G} to increase with slope $\cong 1$ as shown in Figure 6d. Notably, rings at higher densities seem to align slightly more, likely due to spatial restrictions suppressing tumbling more completely.

The alignment behavior of semiflexible rings is intuitive, but it is still instructive to consider the implications especially in the context of the alignment of stacks under weak shear as presented in Figure 3b,c. When thinking back to the angle $\langle\phi\rangle$ of stack to flow axis from Figure 3b, we learned that stacks orient themselves with increasing shear before they eventually break apart. The angle $\langle\xi\rangle$ of a stack to individual directors on that stack, however, follows a reverse trend (see Figure 3c): rings orient more orthogonal to the stack they belong to the more the stack tilts, and this trend continues until individual rings do not align any further despite the imposed shear. At the onset of regime C, $\langle\xi\rangle$ starts to decrease again, while $\langle\phi\rangle$ shoots up. Knowing that, at this stage, rings are oriented parallel to each other (Figure 4) and into the flow-vorticity plane (Figure 7), they can slide on top of each other, and the stacks break. We suggest this mechanism is at the heart of the breaking of clusters, and its absence in regime B is what allows clusters to be reoriented in a stable fashion.

Additional configurations of individual rings can be seen in Supporting Videos S6−S13 for flow-gradient and flow-vorticity perspectives and different shear rates and densities. Particularly instructive is a comparison between Supporting Videos S6 and S7 (individual rings at low bulk density and high shear) to Supporting Videos S12 and S13 (individual rings at high bulk density and high shear), as well as the progression with increasing shear rates at constant bulk density in Supporting Videos S8−S13.

3.5. Memory of Sheared Cluster Glasses. Since glasses are inherently nonequilibrium structures, it is not necessarily true that, once they are subjected to shear and after the cessation of the latter, the system is going to return to its state before shear was applied. It is possible that the system displays memory of the applied shear, which thus introduces permanent or at least long-lived structural changes into the system. To investigate this scenario for the sheared cluster glasses at hand, we performed additional simulations at $\rho^* \cong 26.36$ in which we stopped the shear and monitored the relaxation dynamics of the system and the state it reached after shear cessation. Here, we disregarded HI, since we have shown before that consideration or disregard of HI reproduces a qualitatively identical behavior at the investigated densities. It indeed appears that sheared cluster glasses have memory and maintain some of the parameters influenced and altered by shear when equilibrium is restored, and this behavior seems to be dependent on shear rate. A selection of relevant parameters is presented in Figure 8.

The dispersion index relaxes rather well (Figure 8a), indicating consistent clustering behavior independent of the

https://dx.doi.org/10.1021/acsapm.0c00522
ACS Appl. Polym. Mater. 2020, 2, 3505−3517

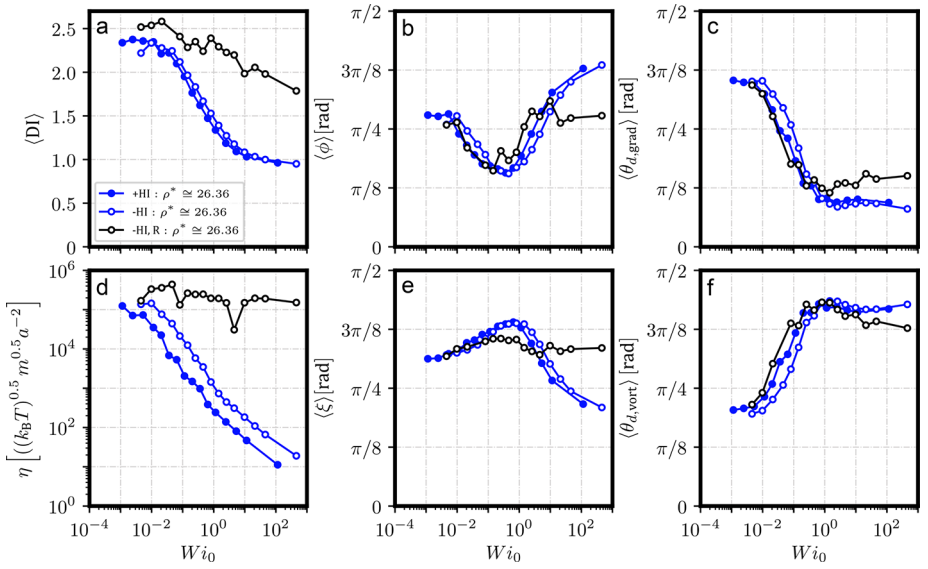

Figure 8. Relaxation behavior of sheared cluster glasses at $\rho^* \cong 26.36$. Comparison of regular shear runs (blue) with relaxation from shear (black), with (●) and without (○) HI. If the system did not have any memory, all black data points should collapse onto the same horizontal line, matching the equilibrium value. All panels show data against increasing Weissenberg number Wi_0. For the relaxation-from-shear runs, Wi_0 indicates the imposed shear rate prior to equilibration. (**a**) Dispersion Index ⟨DI⟩, compare Figure 3a. (**b**) Average angle $\langle\phi\rangle$ of regression fit through all centers-of-mass on a stack to flow axis, compare Figure 3b. (**c**) Average angle $\langle\theta_{\mathrm{d,\,grad}}\rangle$ of ring directors to gradient axis, compare Figure 7b. (**d**) Polymeric viscosity η, compare Figure 5. (**e**) Average angle $\langle\xi\rangle$ of regression fit through all centers-of-mass on a stack to individual directors of rings on that stack, compare Figure 3c. (**f**) Average angle $\langle\theta_{\mathrm{d,vort}}\rangle$ of ring directors to vorticity axis, compare Figure 7c.

starting configuration. The deviation from its equilibrium value for initial high shear stems from the long relaxation time τ of the system, and we expect it to equilibrate fully given sufficient time. This is also evidenced by Supporting Videos S14−S17, indicating regular clustering behavior. Similarly, the polymeric viscosity η relaxes well (Figure 8d), especially since our approach can cause its value to fluctuate a bit for very low shear rates.

The overall orientation of rings and clusters, however, has significant memory (Figure 8b,c,e,f). On the one hand, the orientation angle of stacks to the flow axis $\langle\phi\rangle$ does not relax for originally weak shear rates (Figure 8b), where values match the regular shear data almost perfectly. For originally strong shear rates, on the other hand, the equilibrium values are matched upon relaxation. As stated earlier, stacks under weak shear align with the flow direction, a feature that appears to be maintained upon subsequent equilibration. This behavior is different for originally strong shear, where stacks have been broken completely and the rings are distributed randomly. Such a system is bound to relax just as a regularly initialized system would. The overall angle $\langle\xi\rangle$ of ring directors to the stack they belong to relaxes nicely across shear rates (Figure 8e). Individual rings, no longer forced to align into the flow-vorticity plane, are free to reorient themselves in a way that is spatially favorable. Note, however, that this parameter is susceptible to changes in stack length. Further evidence for our predictions is provided by Supporting Videos S14−S17.

Lastly, the overall average angles $\langle\theta_{\mathrm{d}}\rangle$ of directors to gradient (Figure 8c) and vorticity axes (Figure 8f) do not relax at all. We suggest that, while rings are free to match the orientation of their stacks, their individual average orientation does not change from whichever the priorly imposed shear dictated. From Figure 8 and Supporting Videos S14−S17, we can conclude that sheared cluster glasses relax into different configurations depending on the priorly imposed shear rate. It appears feasible, then, to use shear as a means of manipulating the overall structure of a cluster glass and, perhaps, its conductive properties through deliberate alignment of stacks in a certain direction.

4. CONCLUSIONS

In this work, we have investigated the shear response of a cluster glass formed by semiflexible ring polymers to externally imposed shear. We have identified three regimes in the response of the system to its flow: at very low shear rates, the system flows while maintaining its equilibrium structure. For weak to moderate shear rates, we have observed stacks of rings that had formed in equilibrium to realign themselves under shear, and for all rings on a given stack to align themselves into the flow-vorticity plane as much as possible. Under strong shear, the stacks get destroyed, and all rings are distributed homogeneously as they flow, but their individual alignment still holds true. The result is shear thinning across all investigated ranges of $\dot{\gamma}$ or Wi_0. The ability to control the size and orientation of the clusters through the application of shear and the memory of the collectively reoriented clusters after the application and cessation of shear opens up the possibility for the creation of anisotropic materials with controlled porosity and tunable mechanical and transport properties.

Future investigations should consider the effect of mixing linear chains into this system, as well as try to predict the resulting equilibrium orientational bias for stacks of rings after the system has been sheared. If it is indeed possible to influence the orientation of ring clusters through shear even after the system has been restored back to equilibrium, it might be possible to extrapolate this knowledge onto different flows and topologies and make use of it in other systems modeled by semiflexible rings. Studies toward these aims are currently in the works.

https://dx.doi.org/10.1021/acsapm.0c00522
ACS Appl. Polym. Mater. 2020, 2, 3505−3517

■ ASSOCIATED CONTENT

Supporting Information

The Supporting Information is available free of charge at https://pubs.acs.org/doi/10.1021/acsapm.0c00522.

- Detailed methods of both computational and analytical nature (PDF)
- Stack-colored centers-of-mass of rings, flow-gradient view, $Wi_0 \cong 4.55 \times 10^{-3}$. -HI, $\rho^* \cong 26.36$. Video includes a time range of 24.14 $\tau_{R,0}$ after initial warmup (MPG)
- Stack-colored centers-of-mass of rings, flow-gradient view, $Wi_0 \cong 4.55 \times 10^{-2}$. -HI, $\rho^* \cong 26.36$. Video includes a time range of 55.37 $\tau_{R,0}$ after initial warmup (MPG)
- Stack-colored centers-of-mass of rings, flow-gradient view, $Wi_0 \cong 4.55 \times 10^{-1}$. -HI, $\rho^* \cong 26.36$. Video includes a time range of 56.30 $\tau_{R,0}$ after initial warmup (MPG)
- Stack-colored centers-of-mass of rings, flow-gradient view, $Wi_0 \cong 4.55 \times 10^{0}$. -HI, $\rho^* \cong 26.36$. Video includes a time range of 56.41 $\tau_{R,0}$ after initial warmup (MPG)
- Stack-colored centers-of-mass of rings, flow-gradient view, $Wi_0 \cong 4.55 \times 10^{1}$. -HI, $\rho^* \cong 26.36$. Video includes a time range of 54.70 $\tau_{R,0}$ after initial warmup.(MPG)
- Single ring extracted from bulk simulation, flow-gradient view, $Wi_0 \cong 4.55 \times 10^{1}$. -HI, $\rho^* \cong 0.18$. Video includes a time range of 32.95 $\tau_{R,0}$ after initial warmup (MPG)
- Single ring extracted from bulk simulation, flow-vorticity view, $Wi_0 \cong 4.55 \times 10^{1}$. -HI, $\rho^* \cong 0.18$. Video includes a time range of 32.95 $\tau_{R,0}$ after initial warmup (MPG)
- Single ring extracted from bulk simulation, flow-gradient view, $Wi_0 \cong 4.55 \times 10^{-3}$. -HI, $\rho^* \cong 26.36$. Video includes a time range of 48.77 $\tau_{R,0}$ after initial warmup (MPG)
- Single ring extracted from bulk simulation, flow-vorticity view, $Wi_0 \cong 4.55 \times 10^{-3}$. -HI, $\rho^* \cong 26.36$. Video includes a time range of 48.77 $\tau_{R,0}$ after initial warmup (MPG)
- Single ring extracted from bulk simulation, flow-gradient view, $Wi_0 \cong 4.55 \times 10^{-1}$. -HI, $\rho^* \cong 26.36$. Video includes a time range of 39.76 $\tau_{R,0}$ after initial warmup (MPG)
- Single ring extracted from bulk simulation, flow-vorticity view, $Wi_0 \cong 4.55 \times 10^{-1}$. -HI, $\rho^* \cong 26.36$. Video includes a time range of 39.76 $\tau_{R,0}$ after initial warmup (MPG)
- Single ring extracted from bulk simulation, flow-gradient view, $Wi_0 \cong 4.55 \times 10^{1}$. -HI, $\rho^* \cong 26.36$. Video includes a time range of 52.28 $\tau_{R,0}$ after initial warmup (MPG)
- Single ring extracted from bulk simulation, flow-vorticity view, $Wi_0 \cong 4.55 \times 10^{1}$. -HI, $\rho^* \cong 26.36$. Video includes a time range of 52.28 $\tau_{R,0}$ after initial warmup (MPG)
- Rerelaxation after shearing. Stack-colored centers-of-mass of rings, flow-gradient view, original $Wi_0 \cong 4.55 \times 10^{-2}$. -HI, $\rho^* \cong 26.36$. Video includes a time range of 32.80 $\tau_{R,0}$ after initial warmup (MPG)
- Rerelaxation after shearing. Stack-colored centers-of-mass of rings, flow-gradient view, original $Wi_0 \cong 4.55 \times 10^{-1}$. -HI, $\rho^* \cong 26.36$. Video includes a time range of 32.93 $\tau_{R,0}$ after initial warmup (MPG)
- Rerelaxation after shearing. Stack-colored centers-of-mass of rings, flow-gradient view, original $Wi_0 \cong 4.55 \times 10^{0}$. -HI, $\rho^* \cong 26.36$. Video includes a time range of 32.95 $\tau_{R,0}$ after initial warmup (MPG)
- Rerelaxation after shearing. Stack-colored centers-of-mass of rings, flow-gradient view, original $Wi_0 \cong 4.55 \times 10^{1}$. -HI, $\rho^* \cong 26.36$. Video includes a time range of 32.95 $\tau_{R,0}$ after initial warmup (MPG)

■ AUTHOR INFORMATION

Corresponding Author

Maximilian Liebetreu − *Faculty of Physics, University of Vienna, 1090 Vienna, Austria;* orcid.org/0000-0001-8374-8476; Email: maximilian.liebetreu@univie.ac.at

Author

Christos N. Likos − *Faculty of Physics, University of Vienna, 1090 Vienna, Austria;* orcid.org/0000-0003-3550-4834

Complete contact information is available at: https://pubs.acs.org/10.1021/acsapm.0c00522

Notes

The authors declare no competing financial interest.

■ ACKNOWLEDGMENTS

The simulations presented in this work were performed (in part) on the Vienna Scientific Cluster. M.L. was financially supported by the uni:docs Fellowship Programme of the University of Vienna. The code employed to obtain the results presented in this work is available upon reasonable request to the authors.

■ REFERENCES

(1) Arai, Y.; Yasuda, R.; Akashi, K.; Harada, Y.; Miyata, H.; Kinosita, K., Jr.; Itoh, H. Tying a Molecular Knot with Optical Tweezers. *Nature* **1999**, *399*, 446−448.

(2) Klotz, A. R.; Soh, B. W.; Doyle, P. S. Equilibrium Structure and Deformation Response of 2D Kinetoplast Sheets. *Proc. Natl. Acad. Sci. U. S. A.* **2020**, *117*, 121−127.

(3) An, R.; Li, Q.; Fan, Y.; Li, J.; Pan, X.; Komiyama, M.; Liang, X. Highly Efficient Preparation of Single-Stranded DNA Rings by T4 Ligase at Abnormally Low Mg(II) Concentration. *Nucleic Acids Res.* **2017**, *45*, No. e139.

(4) Hu, L.; Lu, C.-H.; Willner, I. Switchable Catalytic DNA Catenanes. *Nano Lett.* **2015**, *15*, 2099−2103.

(5) Lu, C.-H.; Cecconello, A.; Qi, X.-J.; Wu, N.; Jester, S.-S.; Famulok, M.; Matthies, M.; Schmidt, T.-L.; Willner, I. Switchable Reconfiguration of a Seven-Ring Interlocked DNA Catenane Nanostructure. *Nano Lett.* **2015**, *15*, 7133−7173.

(6) Lu, C.-H.; Cecconello, A.; Willner, I. Recent Advances in the Synthesis and Functions of Reconfigurable Interlocked DNA Nanostructures. *J. Am. Chem. Soc.* **2016**, *138*, 5172−5185.

(7) Ahmadian Dehaghani, Z.; Chubak, I.; Likos, C. N.; Ejtehadi, M. R. Effects of Topological Constraints on Linked Ring Polymers in Solvents of Varying Quality. *Soft Matter* **2020**, *16*, 3029−3038.

(8) Rauscher, P. M.; Schweizer, K. S.; Rowan, S. J.; de Pablo, J. J. Thermodynamics and Structure of Poly[n] catenane Melts. *Macromolecules* **2020**, *53*, 3390−3408.

(9) Li, Y.; Hsiao, K.-W.; Brockman, C. A.; Yates, D. Y.; Robertson-Anderson, R.; Kornfield, J. A.; San Francisco, M. J.; Schroeder, C. M.; McKenna, G. B. When Ends Meet: Circular DNA Stretches Differently in Elongational Flows. *Macromolecules* **2015**, *48*, 5997−6001.

(10) Hsiao, K.-W.; Schroeder, C. M.; Sing, C. E. Ring Polymer Dynamics are Governed by a Coupling between Architecture and Hydrodynamic Interactions. *Macromolecules* **2016**, *49*, 1961−1971.
(11) Liebetreu, M.; Ripoll, M.; Likos, C. N. Trefoil Knot Hydrodynamic Delocalization on Sheared Ring Polymers. *ACS Macro Lett.* **2018**, *7*, 447−452.
(12) Young, C. D.; Qian, J. R.; Marvin, M.; Sing, C. E. Ring Polymer Dynamics and Tumbling-Stretch Transitions in Planar Mixed Flows. *Phys. Rev. E: Stat. Phys., Plasmas, Fluids, Relat. Interdiscip. Top.* **2019**, *99*, 062502.
(13) Soh, B. W.; Klotz, A. R.; Robertson-Anderson, R.; Doyle, P. S. Long-Lived Self-Entanglements in Ring Polymers. *Phys. Rev. Lett.* **2019**, *123*, 048002.
(14) Zhou, Y.; Hsiao, K.-W.; Regan, K. E.; Kong, D.; McKenna, G. B.; Robertson-Anderson, R.; Schroeder, C. M. Effect of Molecular Architecture on Ring Polymer Dynamics in Semidilute Linear Polymer Solutions. *Nat. Commun.* **2019**, *10*, 1753.
(15) Liebetreu, M.; Likos, C. N. Hydrodynamic Inflation of Ring Polymers under Shear. *Commun. Mater.* **2020**, *1*, 4.
(16) Malevanets, A.; Kapral, R. Mesoscopic Model for Solvent Dynamics. *J. Chem. Phys.* **1999**, *110*, 8605−8613.
(17) Halverson, J. D.; Lee, W. B.; Grest, G. S.; Grosberg, A. Y.; Kremer, K. Molecular Dynamics Simulation Study of Nonconcatenated Ring Polymers in a Melt. I. Statics. *J. Chem. Phys.* **2011**, *134*, 204904.
(18) Halverson, J. D.; Lee, W. B.; Grest, G. S.; Grosberg, A. Y.; Kremer, K. Molecular Dynamics Simulation Study of Nonconcatenated Ring Polymers in a Melt. II. Dynamics. *J. Chem. Phys.* **2011**, *134*, 204905.
(19) Halverson, J. D.; Grest, G. S.; Grosberg, A. Y.; Kremer, K. Rheology of Ring Polymer Melts: From Linear Contaminants to Ring-Linear Blends. *Phys. Rev. Lett.* **2012**, *108*, 038301.
(20) Kapnistos, M.; Lang, M.; Vlassopoulos, D.; Pyckhout-Hintzen, W.; Richter, D.; Cho, D.; Chang, T.; Rubinstein, M. Unexpected Power-Law Stress Relaxation of Entangled Ring Polymers. *Nat. Mater.* **2008**, *7*, 997−1002.
(21) Huang, Q.; Ahn, J.; Parisi, D.; Chang, T.; Hassager, O.; Panyukov, S.; Rubinstein, M.; Vlassopoulos, D. Unexpected Stretching of Entangled Ring Macromolecules. *Phys. Rev. Lett.* **2019**, *122*, 208001.
(22) O'Connor, T. C.; Ge, T.; Rubinstein, M.; Grest, G. S. Topological Linking Drives Anomalous Thickening of Ring Polymers in Weak Extensional Flows. *Phys. Rev. Lett.* **2020**, *124*, 027801.
(23) Halverson, J. D.; Smrek, J.; Kremer, K.; Grosberg, A. Y. From a Melt of Rings to Chromosome Territories: the Role of Topological Constraints in Genome Folding. *Rep. Prog. Phys.* **2014**, *77*, 022601.
(24) Smrek, J.; Kremer, K.; Rosa, A. Threading of Unconcatenated Ring Polymers at High Concentrations: Double-Folded vs Time-Equilibrated Structures. *ACS Macro Lett.* **2019**, *8*, 155.
(25) Michieletto, D.; Nahali, N.; Rosa, A. Glassiness and Heterogeneous Dynamics in Dense Solutions of Ring Polymers. *Phys. Rev. Lett.* **2017**, *119*, 197801.
(26) Smrek, J.; Chubak, I.; Likos, C. N.; Kremer, K. Active Topological Glass. *Nat. Commun.* **2020**, *11*, 26.
(27) Weiss, L. B.; Likos, C. N.; Nikoubashman, A. Spatial Demixing of Ring and Chain Polymers in Pressure-Driven Flow. *Macromolecules* **2019**, *52*, 7858−7869.
(28) Weiss, L.; Nikoubashman, A.; Likos, C. N. Topology-Sensitive Microfluidic Filter for Polymers of Varying Stiffness. *ACS Macro Lett.* **2017**, *6*, 1426−1431.
(29) Vinogradov, A. A.; Yin, Y.; Suga, H. Macrocyclic Peptides as Drug Cabdidates: Recent Progress and Remaining Challenges. *J. Am. Chem. Soc.* **2019**, *141*, 4167−4181.
(30) Kaitz, J. A.; Diesendruck, C. E.; Moore, J. S. End Group Characterization of Poly(phthalaldehyde): Surprising Discovery of a Reversible, Cationic Macrocyclization Mechanism. *J. Am. Chem. Soc.* **2013**, *135*, 12755−12761.
(31) Lloyd, E. M.; Lopez Hernandez, H.; Feinberg, A. M.; Yourdkhani, M.; Zen, E. K.; Mejia, E. B.; Sottos, N. R.; Moore, J. S.; White, S. R. Fully Recyclable Metastable Polymers and Composites. *Chem. Mater.* **2019**, *31*, 398−406.
(32) Bernabei, M.; Bacova, P.; Moreno, A. J.; Narros, A.; Likos, C. N. Fluids of Semiflexible Ring Polymers: Effective Potentials and Clustering. *Soft Matter* **2013**, *9*, 1287−1300.
(33) Poier, P.; Likos, C. N.; Moreno, A. J.; Blaak, R. An Anisotropic Effective Model for the Simulation of Semiflexible Ring Polymers. *Macromolecules* **2015**, *48*, 4983−4997.
(34) Poier, P.; Bacová, P.; Moreno, A. J.; Likos, C. N.; Blaak, R. Anisotropic Effective Interactions and Stack Formation in Mixtures of Semiflexible Ring Polymers. *Soft Matter* **2016**, *12*, 4805−4820.
(35) Slimani, M. Z.; Bacova, P.; Bernabei, M.; Narros, A.; Likos, C. N.; Moreno, A. J. Cluster Glasses of Semiflexible Ring Polymers. *ACS Macro Lett.* **2014**, *3*, 611−616.
(36) Moreno, A.; Likos, C. N. Diffusion and Relaxation Dynamics in Cluster Crystals. *Phys. Rev. Lett.* **2007**, *99*, 107801.
(37) Zausch, J.; Horbach, J.; Laurati, M.; Egelhaaf, S. U.; Brader, J. M.; Voigtmann, T.; Fuchs, M. From Equilibrium to Steady State: the Transient Dynamics of Colloidal Liquids under Shear. *J. Phys.: Condens. Matter* **2008**, *20*, 404210.
(38) Vlassopoulos, D.; Cloitre, M. Tunable Rheology of Dense Soft Deformable Colloids. *Curr. Opin. Colloid Interface Sci.* **2014**, *19*, 561−574.
(39) Fuchs, M.; Ballauff, M. Flow Curves of Dense Colloidal Dispersions: Schematic Model Analysis of the Shear-Dependent Viscosity near the Colloidal Glass Transition. *J. Chem. Phys.* **2005**, *122*, 094707.
(40) Siebenbürger, M.; Ballauff, M.; Voigtmann, T. Creep in Colloidal Glasses. *Phys. Rev. Lett.* **2012**, *108*, 255701.
(41) Amann, C. P.; Denisov, D.; Dang, M. T.; Struth, B.; Schall, P.; Fuchs, M. Shear-Induced Breaking of Cages in Colloidal Glasses: Scattering Experiments and Mode Coupling Theory. *J. Chem. Phys.* **2015**, *143*, 034505.
(42) Cloitre, M.; Borrega, R.; Leibler, L. Rheological Aging and Rejuvenation in Microgel Pastes. *Phys. Rev. Lett.* **2000**, *85*, 4819−4822.
(43) Erwin, B. M.; Cloitre, M.; Gauthier, M.; Vlassopoulos, D. Dynamics and Rheology of Colloidal Star Polymers. *Soft Matter* **2010**, *6*, 2825−2833.
(44) Rogers, S. A.; Erwin, B. M.; Vlassopoulos, D.; Cloitre, M. A Sequence of Physical Processes Determined and Quantified in LAOS: Application to a Yield Stress Fluid. *J. Rheol.* **2011**, *55*, 435−458.
(45) Seth, J. R.; Mohan, L.; Locatelli-Champagne, C.; Cloitre, M.; Bonnecaze, R. T. A Micromechanical Model to Predict the Flow of Soft Particle Glasses. *Nat. Mater.* **2011**, *10*, 838−843.
(46) Gompper, G.; Ihle, T.; Kroll, D.; Winkler, R. Multi-Particle Collision Dynamics - a Particle-Based Mesoscale Simulation Approach to the Hydrodynamics of Complex Fluids. *Adv. Polym. Sci.* **2009**, *221*, 1−91.
(47) Kikuchi, N.; Gent, A.; Yeomans, J. M. Polymer Collapse in the Presence of Hydrodynamic Interactions. *Eur. Phys. J. E: Soft Matter Biol. Phys.* **2002**, *9*, 63−66.
(48) Ripoll, M.; Winkler, R. G.; Gompper, G. Hydrodynamic Screening of Star Polymers in Shear Flow. *Eur. Phys. J. E: Soft Matter Biol. Phys.* **2007**, *23*, 349−354.
(49) Lees, A. W.; Edwards, S. F. The Computer Study of Transport Processes under Extreme Conditions. *J. Phys. C: Solid State Phys.* **1972**, *5*, 1921−1929.
(50) Grest, G. S.; Kremer, K. Molecular Dynamics Simulation for Polymers in the Presence of a Heat Bath. *Phys. Rev. A: At., Mol., Opt. Phys.* **1986**, *33*, 3628−3631.
(51) Kremer, K.; Grest, G. S. Dynamics of Entangled Linear Polymer Melts: A Molecular-Dynamics Simulation. *J. Chem. Phys.* **1990**, *92*, 5057−5086.
(52) Verlet, L. Computer Experiments on Classical Fluids. I. Thermodynamical Properties of Lennard-Jones Molecules. *Phys. Rev.* **1967**, *159*, 98−103.
(53) Nickolls, J.; Buck, I.; Garland, M.; Skadron, K. Scalable Parallel Programming with CUDA. *Queue* **2008**, *6*, 40−53.

https://dx.doi.org/10.1021/acsapm.0c00522
ACS Appl. Polym. Mater. 2020, 2, 3505−3517

(54) Tubiana, L.; Rosa, A.; Fragiacomo, F.; Micheletti, C. Spontaneous Knotting and Unknotting of Flexible Linear Polymers: Equilibrium and Kinetic Aspects. *Macromolecules* **2013**, *46*, 3669−3678.
(55) White, J. L. Dynamics of Viscoelastic Fluids, Melt Fracture, and the Rheology of Fiber Spinning. *J. Appl. Polym. Sci.* **1964**, *8*, 2339−2357.
(56) Dealy, J. M. Weissenberg and Deborah Numbers - Their Definition and Use. *Rheology Bulletin* **2010**, *79*, 14−18.
(57) Huang, C. C.; Sutmann, G.; Gompper, G.; Winkler, R. G. Tumbling of polymers in semidilute solution under shear flow. *Europhys. Lett.* **2011**, *93*, 54004.
(58) Rudnick, J.; Gaspari, G. The Asphericity of Random Walks. *J. Phys. A: Math. Gen.* **1986**, *19*, L191−L193.
(59) Poier, P.; Egorov, S. A.; Likos, C. N.; Blaak, R. Concentration-Induced Planar-to-Homeotropic Anchoring Transition of Stiff Ring Polymers on Hard Walls. *Soft Matter* **2016**, *12*, 7983−7994.
(60) Aronovitz, J.; Nelson, D. Universal Features of Polymer Shapes. *J. Phys. (Paris)* **1986**, *47*, 1445−1456.
(61) Bird, R. B.; Hassager, O.; Armstrong, R. C.; Curtiss, C. F. *Dynamics of Polymeric Liquids,* 2nd ed.; John Wiley & Sons: New York, 1987.
(62) Allen, M. P.; Tildesley, D. J. *Computer Simulation of Liquids;* Oxford University Press Inc.: New York, 1987.
(63) Evans, R. M. L.; Haw, M. D. Correlation Length By Measuring Empty Space in Simulated Aggregates. *Europhys. Lett.* **2002**, *60*, 404−410.
(64) Haw, M. D. Void Structure and Cage Fluctuations in Simulations of Concentrated Suspensions. *Soft Matter* **2006**, *2*, 950−956.
(65) Myung, J. S.; Taslimi, F.; Winkler, R. G.; Gompper, G. Self-Organized Structures of Attractive End-Functionalized Semiflexible Polymer Suspensions. *Macromolecules* **2014**, *47*, 4118−4125.
(66) Kam, K. M.; Zeng, L.; Zhou, Q.; Tran, R.; Yang, J. On Assessing Spatial Uniformity of Particle Distributions in Quality Control of Manufacturing Processes. *J. Manuf. Sys.* **2013**, *32*, 154−166.
(67) Humphrey, W.; Dalke, A.; Schulten, K. VMD - Visual Molecular Dynamics. *J. Mol. Graphics* **1996**, *14*, 33−38.
(68) Brader, J. M.; Siebenbürger, M.; Ballauff, M.; Reinheimer, K.; Wilhelm, M.; Frey, S. J.; Weysser, F.; Fuchs, M. Nonlinear Response of Dense Colloidal Suspensions under Oscillatory Shear: Mode-Coupling Theory and Fourier Transform Rheology Experiments. *Phys. Rev. E* **2010**, *82*, 061401.
(69) Sendner, C.; Netz, R. R. Single Flexible and Semiflexible Polymers at High Shear: Non-Monotonic and Non-Universal Stretching Response. *Eur. Phys. J. E: Soft Matter Biol. Phys.* **2009**, *30*, 75−81.
(70) Chen, W.; Chen, J.; Liu, L.; Xu, X.; An, L. Effects of Chain Stiffness on Conformational and Dynamical Properties of Individual Ring Polymers in Shear Flow. *Macromolecules* **2013**, *46*, 7542−7549.

https://dx.doi.org/10.1021/acsapm.0c00522
ACS Appl. Polym. Mater. 2020, 2, 3505−3517